

Highlights

Torsion in a rotating coupled cylinder with different coupling conditions: stress, displacement and approximating a damaged cylinder

Igor Istenes, Daniel Peck, Yuriy Protserov, Natalya Vaysfeld, Zinaida Zhuravlova

- The displacement and stress for a rotating coupled cylinder under torsion are obtained.
- The impact of cylinder geometry, composition, and rotation rate are investigated.
- The impact of differing contact conditions: ideal, soft or rigid, is investigated.
- A method for approximating cylinder damage using a weak interfacial layer is outlined, with application to non-destructive testing.

Torsion in a rotating coupled cylinder with different coupling conditions: stress, displacement and approximating a damaged cylinder

Igor Istenes^a, Daniel Peck^b, Yuriy Protserov^c, Natalya Vaysfeld^{b,d}, Zinaida Zhuravlova^c

^a*Roez R&D, Bratislava, 811 04, Slovakia*

^b*Department of Mathematics, Aberystwyth University, Aberystwyth, SY23 3BZ, Wales, United Kingdom*

^c*Odesa I.I. Mechnikov National University, Faculty of Mathematics, Physics and Information Technologies, str. Dvoryanska, 2, Odesa, 65082, Ukraine*

^d*King's College London, London, S2.35, United Kingdom*

Abstract

The torsion loading of a coupled cylinder, whose distinct upper and lower cylindrical sections may be composed of different materials, is considered. The bottom of the cylinder is fixed in place, and induces the cylinder rotation. The torsion is applied via an arbitrary loading on the upper face. Three forms of coupling condition between the upper and lower cylinders are outlined: ideal, soft (weak), and rigid (hard/ stiff) contact. The resulting displacements and tangential stresses are obtained using the finite Hankel transform, and a Green's function representation of the displacement. Numerical results are provided, and the impact of the differing coupling conditions investigated for a range of cylinder geometries and material properties. A method for using the coupled cylinder model to approximate the displacement of a cylinder containing a damaged region via a weak interfacial layer is outlined. The properties of the weak interface layer needed for this approximation are determined, and the advantages of its use in non-destructive testing are discussed.

Keywords: torsion problem, elastic cylinder, coupled cylinders, soft

URL: igor.istenes@roez.sk (Igor Istenes), dtp@aber.ac.uk (Daniel Peck), protserov@onu.edu.ua (Yuriy Protserov), natalya.vaysfeld@kcl.ac.uk (Natalya Vaysfeld), z.zhuravlova@onu.edu.ua (Zinaida Zhuravlova)

contact, rigid contact, ideal contact.

1. Introduction

Torsion problems are those in which a torque is applied, either to the top or sides of an object, which causes deformation as a twisting motion. The study of torsion in coupled or layered elastic cylinders, encompassing both solid and hollow geometries, is a cornerstone for understanding the mechanics of coupled fields in layered composite structures. Such analyses are critical for advancing engineering applications ranging from structural components in aerospace and civil engineering (turbines, etc), to biomedical implants (to account for movement of the neck/ spine/ joints) and soft robotics (for use in actuators, etc), amongst others. The unique mechanical responses induced by layered construction, combined with the constraints of finite dimensions, introduce complex interactions that require advanced modelling techniques and computational tools. The problem of torsion in layered cylinders not only presents theoretical interest but also bears practical relevance due to the widespread application of layered composite materials in industrial practices.

Over recent decades, significant progress has been made in developing analytical, semi-analytical, and numerical approaches to model torsion in finite elastic cylinders. Classical solutions, such as those based on Saint-Venant's principle, have been adapted and extended to account for the intricacies introduced by layered structures. Moreover, computational methods, including finite element analysis (FEA) and boundary element methods (BEM), have become essential tools in handling the multi-layered configurations and heterogeneous material properties of these cylinders. Recently, researchers have explored machine learning techniques to optimize model parameters and to simulate complex scenarios, signaling a shift toward hybridized approaches that combine traditional mechanics with data-driven insights.

The problem for a multilayered elastic finite cylinder with a fixed bottom face and axisymmetric tangent stress applied to its lateral surface was solved for an arbitrary number of layers in Protserov and Vaysfeld (2017), while the elastodynamic solution for the case without a fixed bottom face was provided in Wang and Gong (1992). The problem of a cylindrical interface crack in a bi-layered tubular composite of finite thickness under torsion was investigated in Li et al. (2013) with the help of the methods of Fourier integral transform and Cauchy singular integral equations. An exact analytical solution to the problem of large deformations of a multilayer cylindrical rod under

multistage deformation was obtained in Zingerman et al. (2023) for incompressible isotropic nonlinear elastic materials. The effect of torsion-loading on similarly nonlinear rubber cylinders was considered in Falope et al. (2025). A finite elastic cylinder, either hollow or solid, was considered in Vaysfeld and Protcerov (2017), where a system of N ring-shaped cracks was situated inside the cylinder parallel to the cylinder's axis. This was extended to cover a ring-crack within a hollow cylinder under torsion in Zhuravlova et al. (2024). The torsional wave dispersion in pre-stressed compound bi-material solid and hollow cylinders was studied in Akbarov et al. (2011). The investigations was made within the scope of the three-dimensional linearized theory of elastic waves in initially stressed bodies. This work was extended to cover imperfect contact, assuming a shear-spring type continuity condition, in Akbarov et al. (2025). Exact solutions were presented in Kuo and Conway (1973) for the Saint-Venant torsion of circular tubes and solid cylinders which were reinforced by cylindrical inclusions of different material equally spaced around a concentric circle. More recently, the case of pressurised cylindrical segments (shells) comprised of saturated porous media was given in Esfandyari and Nejad (2025).

Meanwhile, in Akhmedov and Ustinov (2009) the structure of the boundary layer when consider torsion of a radially stratified spherical shell with an arbitrary number of alternating hard and soft layers was investigated. They established that the type of contact between layers - whether ideal, soft, or rigid (hard) - greatly influences how stresses and deformations propagate through the structure. These differing types of contact describe the coupling between the cylinder layers, whether they are directly bonded or with some interfacial layer between them, which can either enhance or reduce the cylinder's overall mechanical performance depending on the application Mishuris et al. (2006). A three-dimensional unilateral contact problem for thin viscoelastic layers bonded to rigid substrates shaped like elliptic paraboloids was considered in Argatov and Mishuris (2011), where two cases were studied: one where the layers were compressible (both had Poisson's ratio $\nu \ll 0.5$), and another where the layer materials are incompressible ($\nu = 0.5$). The case of interlayer sliding between an elastic half-plane and attached coating was examined in Mikhasev and Eremeyev (2024). There, sliding was introduced by assuming that the interfacial shear stresses are linearly related to the relative displacement of the layers, with the coefficient given by some new constant called the bond stiffness. This bond stiffness was found to significantly effect the resulting phase velocity of antiplane waves within the system. The

case of a radially layered piezoelectric-dielectric solid cylinder incorporating surface-interface effects was investigated in Dhua et al. (2025). They found that the impact of these surface-interface effects on shear waves depended on the size of the interface layer. Similar recent efforts by Dastjerdi et al. (2025) determined the displacement within a smart piezomagnetic-flexomagnetic-elastic disc under combined magneto-mechanical loading. New variational principles and bounds were introduced in Lipton and Vernescu (1996), describing the effective conductivity tensor for anisotropic two-phase heat conducting composites with interfacial surface resistance between phases, where the new upper bound is given in terms of the two-point correlation function, component volume fractions and moment of inertia tensor for the surface of each heterogeneity. The asymptotic scheme for the analysis of dilute elastic composites, which includes circular inclusions with imperfect bonding at the interface, was presented in Bigoni et al. (1998). In that work, the interface was characterized by a discontinuous displacement field across it which was linearly related to the tractions. Imperfect transmission conditions were evaluated in the case of a weakly compressible elastic interphase between different bonded elastic materials in Mishuris (2004a). It was shown that the corresponding transmission conditions differed from those with a compressible elastic interface. The Mode III problem for an interface crack tip lying at various nonideal (imperfect) interfaces in a dissimilar elastic body was investigated in Mishuris (2004b), and nonclassical transmission conditions described by the features of a thin nonhomogeneous anisotropic elastic layer situated between the material layers was discussed.

These results and investigations make it clear that the interface can play a significant role in determining system behaviour. In practice, three types of contact are primarily assumed: ideal, soft, or rigid (hard) contact.

Ideal contact between layers assumes a perfect, uninterrupted bond across the entire interface, with no slippage or separation between layers. Under ideal contact conditions, layers act as a unified structure, allowing stresses and strains to distribute evenly throughout the entire cylinder. This type of bonding maximizes torsional rigidity and structural integrity, making it especially advantageous in high-stress applications such as aerospace shafts or structural supports, where uniform stress distribution is crucial. However, ideal contact is challenging to achieve in practice, particularly with composite materials or under thermal cycling, which can cause differential expansion and lead to stress concentration.

Soft contact, in contrast, allows for some degree of slippage or relative

movement between layers. This type of contact is often characterized by a compliant interface, such as a thin, flexible bonding layer or interfacial adhesive that permits minor displacements. Soft contact can absorb and dissipate energy, making it beneficial in applications where damping or vibration reduction is desired, such as in automotive components and noise-sensitive environments. Additionally, soft contacts can accommodate differences in thermal expansion between layers, reducing the risk of delamination under temperature changes. However, the allowance for movement at the interface typically results in lower torsional rigidity, as the layers no longer function as a single, cohesive unit.

Rigid contact (sometimes called hard or stiff contact) provides a rigid bonding interface, but unlike ideal contact, it does not assume perfect adhesion across the entire interface. Instead, hard contact allows for some normal force transfer but restricts any lateral or tangential movement between layers. This type of contact maintains significant torsional and bending rigidity while still tolerating slight inconsistencies or material mismatches at the interface. In applications such as drill rods, turbine components, or mechanical couplings, hard contact is often used to maintain high stiffness and resistance to shear without requiring the perfect bonding assumed in ideal contact. However, rigid contact can introduce localized stress concentrations and is more prone to interfacial fracture if the cylinder is subjected to extreme mechanical or thermal loading.

Integrating these types of contact into torsion problem models, via the boundary conditions between a cylinder's sections, highlights how the level of bonding can be selected to meet specific functional requirements in engineering applications. Ideal contact maximizes structural integrity, making it suitable for applications requiring high rigidity and uniform stress transfer. Soft contact is useful for applications that need energy dissipation or thermal flexibility, while rigid contact strikes a balance, offering high stiffness with some tolerance to interfacial stress. The primary motive for this work therefore is to understand, both qualitatively and quantitatively, the mechanics and trade-offs associated with each type of contact in joined hollow cylinders. This understanding is essential for designing connected cylindrical sections that meet the diverse demands of fields like aerospace, automotive, and biomedical engineering.

In this paper we consider a two-sectioned hollow cylinder under torsion loading on the top face. The cylinder is assumed to be rotating, achieved by fixing it at bottom end, to facilitate application to turbines and similar

processes. The three primary types of contact condition: ideal, soft and rigid, are all considered. A complete description of the cylinders displacement and tangential stress are determined. This allows for a thorough investigation into the impact of the choice of interface, and the differing behaviour between them.

The paper is organised as follows. First the problem of coupled hollow cylinders is formally stated in Sect. 2. The governing equations are provided, and the various contact conditions outlined. Next, in Sect. 3 we introduce the modified finite Hankel transform, which will be used to solve the system and obtain the displacement. The transforms definition and properties are provided, the transformed equations stated, and the Green's function for the problem derived. The end result is an expression for the displacement in terms of the Green's function, with some unknown terms. In Sect. 4, an explicit expression for the displacement in each of the differing contact scenarios is obtained. This is used to provide numerical results in Sect. 5. The impact of the interface type is investigated, as well as its dependence on the cylinder geometry, material composition, and the rotation frequency. This model is then used in Sect. 6 to investigate approximating damage within a single cylinder, for example the presence of a ring crack, using a weak interfacial layer. It is shown that the shear modulus of this layer needed for an effective approximation can be easily obtained from a linear relation between the shear modulus and the arithmetic mean of the displacements (observed/ ideal). Finally, concluding remarks are provided in Sect. 7.

2. Problem statement

2.1. The coupled cylinder

We consider the case of a coupled hollow cylinder, whose distinct upper and lower sections are connected by some interfacial layer, as depicted in Fig. 1. The system is considered in cylindrical coordinates (r, ϕ, z) . The cylinder is assumed to be rotating at some frequency ω . The two sections both have inner radius a and outer radius R , giving the problem radial coordinate $a < r < R$. They are axisymmetric about the angle $-\pi < \phi < \pi$. The lower cylinder covers height $0 < z < h$, with shear modulus μ_1 and density ρ_1 . The upper cylinder covers height $h + h_0 < z < H$ and has shear modulus μ_2 and density ρ_2 , where h_0 is the height of the interface between the two cylindrical sections. Throughout this paper we will denote the lower section using indices $k = 1$, and upper cylinder $k = 2$. A coupling condition

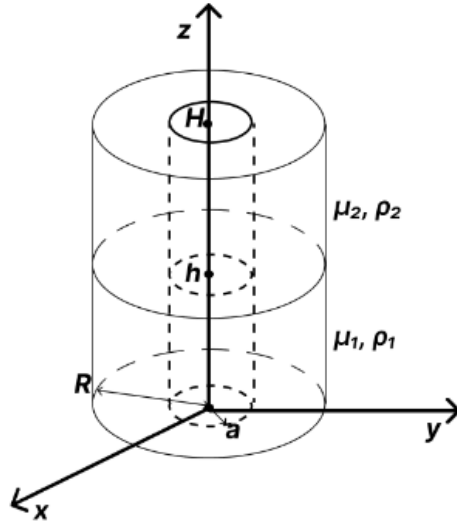


Figure 1: Geometry and coordinate system of two-layered hollow cylinder.

describes the contact between the two sections, with the three considered cases (ideal, soft and rigid contact) being outlined in Sect. 2.2.

It is assumed that the cylindrical surfaces are free from load

$$\tau_{r\phi}^{(k)} \Big|_{r=a,R} = \mu_k \left(\frac{\partial u_k}{\partial r} - \frac{1}{r} u_k \right) \Big|_{r=a,R} = 0, \quad k = 1, 2, \quad (1)$$

where $\tau_{r\phi}^{(k)}(r, z)$, $u_k(r, z)$, are the tangential stress and displacement of each section $k = 1, 2$.

The bottom boundary of the cylinder is fixed in place, while an axisymmetric tangential torsion loading is applied to the upper face

$$u_1(r, 0) = 0, \quad \tau_{z\phi}^{(2)} \Big|_{z=H} = p(r)e^{i\omega t}, \quad (2)$$

where ω is a frequency of the cylinders rotation, $p(r)$ is a prescribed function, and t is time. Note that this temporal term is only introduced to ensure we describe a steady-state system, and the resulting displacement will be independent of time.

The equation of motion describing the displacement u_k in each section $k = 1, 2$ of the rotating cylinder is given by Popov et al. (1999)

$$\frac{1}{r} \frac{\partial}{\partial r} \left(r \frac{\partial u_k}{\partial r} \right) - \frac{1}{r^2} u_k + \frac{\partial^2 u_k}{\partial z^2} + \frac{\omega^2}{c_k^2} u_k = 0, \quad k = 1, 2, \quad (3)$$

where $c_k = \sqrt{\mu_k \rho_k^{-1}}$, $k = 1, 2$, are shear wave speeds.

Note that in the case with $\omega = 0$ expression (3) reduces to the Laplacian, and the model can be altered to describe heat flux in a coupled cylinder, such as those used when drilling wells for geothermal energy extraction.

2.2. Coupling of the two layers

We consider three types of coupling conditions between the cylinder sections: ideal contact, soft (weak) contact, and rigid (hard/ stiff) contact. The boundary formulation for this coupling needs to be defined in order to construct the general solution of the boundary value problem (1)-(3). We therefore outline the three distinct couplings below.

2.2.1. Ideal contact

The case of ideal contact assumes perfect coupling between the two cylinder sections, such that the displacement u_k and tangential torsion $\tau_{z\phi}^{(k)}$ of the two sections $k = 1, 2$ at the boundary are identical. The ideal contact conditions between the sections can therefore be described in terms of the jump $\llbracket \cdot \rrbracket$ as

$$\llbracket u_k(r, h) \rrbracket = u_2(r, h+0) - u_1(r, h-0) = 0, \quad (4)$$

$$\llbracket \tau_{z\phi}^{(k)}(r, h) \rrbracket = \tau_{z\phi}^{(2)}(r, h+0) - \tau_{z\phi}^{(1)}(r, h-0) = \mu_2 \left. \frac{\partial u_2}{\partial z} \right|_{z=h+0} - \mu_1 \left. \frac{\partial u_1}{\partial z} \right|_{z=h-0} = 0.$$

2.2.2. Soft contact

The case of soft (weak) contact assumes that there exists some thin interface between the upper and lower sections, which is significantly weaker than the cylindrical layers themselves. The interface is therefore defined by its density ρ_0 , its height $h_0 \ll H$ (the interface is thin), and its shear modulus $\mu_0 \ll \mu_k$, $k = 1, 2$ (it is constructed of a soft material). An example of such an interface would be the use of a weak adhesive which deforms but maintains its integrity through the process, or a layer added to provide energy/ thermal dissipation.

The contact conditions for such a thin “soft” interface are provided in Mishuris (2004a). It is assumed that there is continuity of the stress function over the interface, while the jump of displacements is supposed proportional to the stress

$$\llbracket u_k(r, h) \rrbracket = K_1 \left. \frac{\partial u_2}{\partial z} \right|_{z=h+0}, \quad \llbracket \tau_{z\phi}^{(k)}(r, h) \rrbracket = 0, \quad (5)$$

where $K_1 = \mu_2 \mu_0^{-1} h_0$.

2.2.3. Rigid contact

The case of rigid (hard/ stiff) contact assumes that the two cylindrical sections are coupled via some significantly stronger interface layer. The interface is again defined by its density ρ_0 , its height $h_0 \ll H$ (the interface is thin), and its shear modulus $\mu_0 \gg \mu_k$, $k = 1, 2$ (the interface is strong/ rigid). Examples of rigid contact would include the bonding of a metal layer between rubber sections, as used in some wheel designs.

The contact conditions for such a rigid interface are provided in Mishuris (2004a). The displacements across the interface are assumed to be continuous, such that the displacement jump is zero.

$$\llbracket u_k(r, h) \rrbracket = 0. \quad (6)$$

Meanwhile, the equation of motion for the interfacial layer takes the form

$$\frac{1}{r} \frac{d}{dr} \left(r \frac{dv(r)}{dr} \right) - \frac{1}{r^2} v(r) + \frac{1}{\mu_0 h_0} \left(\mu_2 \frac{\partial u_2}{\partial z} \Big|_{z=h+0} - \mu_1 \frac{\partial u_1}{\partial z} \Big|_{z=h-0} \right) + \frac{\omega^2}{c_0^2} v(r) = 0, \quad (7)$$

where $v(r)$ is displacement of the interface, and $c_0 = \sqrt{\mu_0 \rho_0^{-1}}$.

It is also assumed that the cylindrical surfaces of the interface are free from stress

$$\tau_{r\phi}^{(0)} \Big|_{r=a,R} = \mu_0 \left[\frac{dv(r)}{dr} - \frac{1}{r} v(r) \right] \Big|_{r=a,R} = 0, \quad (8)$$

where $\tau_{r\phi}^{(0)}$ is the tangential stress of the rigid interface.

3. The deriving of a solution in the transform's domain

With the problem geometry and interface conditions outlined, we now seek to obtain a unique expression for the displacements u_k , $k = 1, 2$, for each case. This will be achieved by first applying the finite Hankel transform, whose definition and properties are outlined in Sect. 3.1. Applying this transform eliminates the variable r , with the reduction of the transformed system to a one dimensional boundary value problem provided in Sect. 3.2. This transformed problem can then be solved in terms of a 1D Green's function, which is obtained in Sect. 3.3.

3.1. The finite Hankel transform

In order to reduce the problem (1)-(3) to a one dimensional boundary value problem, we utilize a variant of the finite Hankel transform, defined as (see e.g. Pathak and Singh (1982); Martynenko and Pustilnikov (1996)):

$$u_{kn}(z) = \int_a^R u_k(r, z) K(\lambda_n, r) r dr, \quad k = 1, 2, \quad n \in \mathbb{N}_0, \quad (9)$$

with the kernel

$$K(\lambda_n, r) = J_2(\lambda_n a) Y_1(\lambda_n r) - Y_2(\lambda_n a) J_1(\lambda_n r),$$

where $J_{1,2}(\cdot)$, $Y_{1,2}(\cdot)$ are Bessel functions of the first and second kind respectively (see e.g. Korenev (2002)), and λ_n are nonnegative roots of the transcendental equation Pathak and Singh (1982)

$$J_2(\lambda a) Y_2(\lambda R) - Y_2(\lambda a) J_2(\lambda R) = 0.$$

It is necessary to underline that due to the special boundary conditions (1) $\lambda_0 = 0$ is also an eigenvalue with the corresponding eigenfunction $y_0(r) = r$ and norm Pathak and Singh (1982)

$$\|y_0(r)\|^2 = \int_a^R r^2 \cdot r dr = \frac{R^4 - a^4}{4}.$$

When applied to the governing equation (3), the finite Hankel transform reduces it to a 1D problem due to the following result

$$\int_a^R \left[\frac{\partial}{\partial r} \left(r \frac{\partial u_k}{\partial r} \right) - \frac{1}{r} u_k \right] K(\lambda_n, r) dr = \lambda_n^2 u_{kn}(z), \quad (10)$$

which follows from taking integration by parts and utilizing the properties of Bessel functions (see e.g. Korenev (2002)).

Once the solution of the transformed problem is obtained, the original system is recovered utilizing the inverse finite Hankel transform as

$$u_k(r, z) = \frac{4r}{R^4 - a^4} u_{k0}(z) + \sum_{n=1}^{\infty} u_{kn}(z) \frac{K(\lambda_n, r)}{\|K(\lambda_n, r)\|^2}, \quad (11)$$

where

$$\|K(\lambda_n, r)\|^2 = \int_a^R K^2(\lambda_n, r) r dr = \frac{R^2}{2} K^2(\lambda_n, r) - \frac{2}{\pi^2 \lambda_n^2}, \quad n \in \mathbb{N}.$$

3.2. The transformed problem

With the finite Hankel transform introduced, we apply it to the governing equations and contact conditions for the system. This will yield a transformed problem that we can more easily solve.

3.2.1. The governing equations

Applying the finite Hankel transform (9) to the governing system of equations (1)-(3), noting (10), yields

$$\begin{cases} u''_{kn}(z) - \gamma_{kn}^2 u_{kn}(z) = 0, & 0 < z < H, \quad z \neq h, \\ u_{1n}(0) = 0, \quad u'_{2n}(H) = \mu_2^{-1} p_n, \end{cases} \quad (12)$$

where $n \in \mathbb{N}_0$ and

$$\gamma_{kn}^2 = \lambda_n^2 - \frac{\omega^2}{c_k^2}, \quad p_n = \int_a^R p(r) K(\lambda_n, r) r \, dr.$$

While this provides the transformed system for all $n \in \mathbb{N}_0$, in the following analysis it is useful to take advantage of the known $\lambda_0 = 0$ and consider the case $n = 0$ separately. Evaluating (12) for $n = 0$ gives

$$\begin{cases} u''_{k0}(z) + \beta_k^2 u_{k0}(z) = 0, & 0 < z < H, \quad z \neq h, \\ u_{10}(0) = 0, \quad u'_{20}(H) = \mu_2^{-1} p_0, \end{cases} \quad (13)$$

where

$$\beta_k^2 = \frac{\omega^2}{c_k^2}, \quad p_0 = \int_a^R p(r) r^2 \, dr,$$

where we have used that $K(0, r) = y_0(r) = r$.

This is part of the transformed system that we seek to solve. The remainder will come from the form of the contact condition between the two cylinders.

3.2.2. The coupling conditions

Alongside transforming the governing equations, we must also transform the coupling conditions for the three types of contact being considered. Let us handle each of these separately.

Ideal contact: In transform's domain (9) the conditions (4) take the form

$$\llbracket u_{kn}(h) \rrbracket = 0, \quad \llbracket u'_{kn}(h) \rrbracket = \frac{\mu_1 - \mu_2}{\mu_1} u'_{2n}(h+0), \quad n \in \mathbb{N}_0. \quad (14)$$

Soft contact: The coupling conditions (5) in transform's domain (9) have the following form

$$\llbracket u_{kn}(h) \rrbracket = K_1 u'_{2n}(h+0), \quad \llbracket u'_{kn}(h) \rrbracket = \frac{\mu_1 - \mu_2}{\mu_1} u'_{2n}(h+0), \quad n \in \mathbb{N}_0. \quad (15)$$

Rigid contact: Applying the finite Hankel transform (9) to the coupling conditions for rigid contact (6)-(8) yields the transformed conditions

$$\llbracket u_{kn}(h) \rrbracket = 0, \quad n \in \mathbb{N}_0, \quad \llbracket u'_{kn}(h) \rrbracket = \frac{\mu_1 - \mu_2}{\mu_1} u'_{2n}(h+0) + \frac{\mu_0 h_0 \gamma_{0n}^2}{\mu_1} v_n, \quad n \in \mathbb{N}_0, \quad (16)$$

where $\beta_0^2 = \frac{\omega^2}{c_0^2}$, and $\gamma_{0n}^2 = \lambda_n^2 - \beta_0^2$. In order to maintain coupling of the displacement between the two cylinders and the rigid layer, it is supposed that

$$u_{1n}(h-0) = u_{2n}(h+0) = v_n.$$

Consequently, again treating the case $n = 0$ separately, the second condition in (16) can be rewritten in the form

$$\begin{aligned} \llbracket u'_{k0}(h) \rrbracket &= \frac{\mu_1 - \mu_2}{\mu_1} u'_{20}(h+0) - K_2 \beta_0^2 u_{20}(h+0), \\ \llbracket u'_{kn}(h) \rrbracket &= \frac{\mu_1 - \mu_2}{\mu_1} u'_{2n}(h+0) + K_2 \gamma_{0n}^2 u_{2n}(h+0), \quad n \in \mathbb{N}, \end{aligned} \quad (17)$$

where $K_2 = \mu_0 h_0 \mu_1^{-1}$.

With these conditions obtained, we are now in a position to begin solving the transformed problem. This is achieved by considering the Green's function associated for the boundary value problem.

3.3. A Green's function representation of the transformed displacement

3.3.1. The Green's function

The Green's function $G_{kn}(z, \eta)$, $k = 1, 2$, $n \in \mathbb{N}_0$, in the transformed domain is the solution of (see e.g. Popov et al. (1999))

$$\begin{cases} \frac{\partial^2 G_{kn}(z, \eta)}{\partial z^2} - \gamma_{kn}^2 G_{kn}(z, \eta) = \delta(z - \eta), & 0 < z, \eta < H, \quad z, \eta \neq h, \\ G_{1n}(0, \eta) = 0, & 0 < \eta < H, \\ \left. \frac{\partial G_{2n}(z, \eta)}{\partial z} \right|_{z=H} = 0, & 0 < \eta < H. \end{cases}$$

This is solved using standard techniques. The resulting fundamental basic system of solutions and Green's function Popov et al. (1999) are then given by

$$\Psi_{0n}(z) = \frac{\cosh(\gamma_{2n}H - \gamma_{kn}z)}{\cosh(\gamma_{2n}H)}, \quad \Psi_{1n}(z) = \frac{\sinh(\gamma_{2n}z)}{\gamma_{2n} \cosh(\gamma_{2n}H)}, \quad (18)$$

$$G_{kn}(z, \eta) = -\frac{1}{\gamma_{kn} \cosh(\gamma_{2n}H)} \begin{cases} \cosh(\gamma_{2n}H - \gamma_{kn}\eta) \sinh(\gamma_{kn}z), & z < \eta, \\ \cosh(\gamma_{2n}H - \gamma_{kn}z) \sinh(\gamma_{kn}\eta), & z > \eta. \end{cases}$$

While the above holds for all $n \in \mathbb{N}_0$, it will again be useful to consider the case $n = 0$ separately. Evaluating (13) for $n = 0$ the fundamental basic system of solutions and Green's function for the problem can be written as

$$\Psi_{00}(z) = \frac{\cos(\beta_2H - \beta_kz)}{\cos(\beta_2H)}, \quad \Psi_{10}(z) = \frac{\sin(\beta_2z)}{\beta_2 \cos(\beta_2H)}, \quad (19)$$

$$G_{k0}(z, \eta) = -\frac{1}{\beta_k \cos(\beta_2H)} \begin{cases} \cos(\beta_2H - \beta_k\eta) \sin(\beta_kz), & z < \eta, \\ \cos(\beta_2H - \beta_kz) \sin(\beta_k\eta), & z > \eta. \end{cases}$$

Expressions (18), (19) provide the Green's function for the problem, however they do not account for the coupling condition at the interface.

3.3.2. Representing the transformed displacement in terms of the Green's function

To incorporate the coupling conditions at the interface $z = h$, we seek to represent the transformed displacement u_{kn} in terms of the Green's function. To determine the proper representation of the transformed displacement, let us consider some of the properties of the Green's function.

It has previously been established (see e.g. Popov et al. (1999)) that the Green's function $G_{kn}(z, \eta)$ has the following discontinuous properties during the transition from the point $z = h - 0$ to the point $z = h + 0$:

- the Green's function is continuous

$$\llbracket G_{kn}(z, h) \rrbracket = 0;$$

- its derivative has the jump equal to 1

$$\llbracket \frac{\partial G_{kn}(z, h)}{\partial z} \rrbracket = 1;$$

- its derivative with respect to variable η has jump equal to -1

$$\llbracket \frac{\partial G_{kn}(z, h)}{\partial \eta} \rrbracket = -1;$$

- the jump of the Green's functions second order mixed derivative is zero

$$\llbracket \frac{\partial^2 G_{kn}(z, h)}{\partial z \partial \eta} \rrbracket = 0.$$

This inspires searching for the problem's solution as a superposition of its continuous and discontinuous parts. Following this approach, the solution of (12), (13) are derived in terms of the jump of the transformed displacements' $\llbracket u_{kn}(h) \rrbracket$ and their derivatives $\llbracket u'_{kn}(h) \rrbracket$ as

$$u_{kn} = \frac{p_n \sinh(\gamma_{2n} z)}{\mu_2 \gamma_{2n} \cosh(\gamma_{2n} H)} + \llbracket u'_{kn}(h) \rrbracket G_{kn}(z, \eta)|_{\eta=h} - \llbracket u_{kn}(h) \rrbracket \frac{\partial G_{kn}(z, \eta)}{\partial \eta} \Big|_{\eta=h}, \quad (20)$$

where $n \in \mathbb{N}$, while for the case $n = 0$

$$u_{k0} = \frac{p_0 \sin(\beta_2 z)}{\mu_2 \beta_2 \cos(\beta_2 H)} + \llbracket u'_{k0}(h) \rrbracket G_{k0}(z, \eta)|_{\eta=h} - \llbracket u_{k0}(h) \rrbracket \frac{\partial G_{k0}(z, \eta)}{\partial \eta} \Big|_{\eta=h}. \quad (21)$$

The form of the Green's function is already known from (18), (19). Meanwhile, the remaining terms $\llbracket u_{kn}(h) \rrbracket$ and $\llbracket u'_{kn}(h) \rrbracket$ need to be computed from the specific contact condition.

4. Obtaining an explicit expression for the displacement

With the form of the displacement specified (20)-(21), all that remains is to obtain the unknown transformed displacement jumps $[[u_{kn}(h)]]$ and $[[u'_{kn}(h)]]$, $k = 1, 2$. We obtain these from the coupling conditions associated with the specified contact condition (14)-(17), before applying the inverse finite Hankel transform (11) to obtain the displacement. We consider each of these separately, with the derivation and result for ideal contact being given in Sect. 4.1, soft contact in Sect. 4.2, and rigid contact in Sect. 4.3.

4.1. The displacement for ideal coupling of the cylinders

Combining the formulas for the displacements (20)-(21) with the ideal contact conditions (14), we obtain the system to be solved for the case of ideal contact

$$u_{kn}(z) = \frac{p_n \sinh(\gamma_{2n} z)}{\mu_2 \gamma_{2n} \cosh(\gamma_{2n} H)} - \frac{\mu_2 - \mu_1}{\mu_1} G_{kn}(z, h) u'_{2n}(h + 0), \quad n \in \mathbb{N}, \quad (22)$$

$$u_{k0}(z) = \frac{p_0 \sin(\beta_2 z)}{\mu_2 \beta_2 \cos(\beta_2 H)} - \frac{\mu_2 - \mu_1}{\mu_1} G_{k0}(z, h) u'_{20}(h + 0), \quad (23)$$

In order to find the unknown values $u'_{2n}(h + 0)$ and $u'_{20}(h + 0)$ the expressions (22)-(23) are differentiated with respect to variable z , and the substitutions $k = 2$ and $z = h + 0$ are made. The resulting linear algebraic equations are then solved to obtain

$$u'_{20}(h + 0) = \frac{p_0 \cos(\beta_2 h)}{\mu_2 \Delta_{20}^I}, \quad u'_{2n}(h + 0) = \frac{p_n \cosh(\gamma_{2n} h)}{\mu_2 \Delta_{2n}^I}, \quad n \in \mathbb{N}, \quad (24)$$

where

$$\Delta_{20}^I = \cos(\beta_2 H) - \frac{\mu_2 - \mu_1}{\mu_1} \sin(\beta_2 h) \sin[\beta_2 (H - h)],$$

$$\Delta_{2n}^I = \cosh(\gamma_{2n} H) + \frac{\mu_2 - \mu_1}{\mu_1} \sinh(\gamma_{2n} h) \sinh[\gamma_{2n} (H - h)], \quad n \in \mathbb{N}.$$

Inserting into (22)-(23), we obtain the explicit expressions for the transformed displacements

$$u_{kn}(z) = \frac{p_n \sinh(\gamma_{2n} z)}{\mu_2 \gamma_{2n} \cosh(\gamma_{2n} H)} - \frac{\mu_2 - \mu_1}{\mu_1} \frac{p_n \cosh(\gamma_{2n} h)}{\mu_2 \Delta_{2n}^I} G_{kn}(z, h), \quad n \in \mathbb{N}, \quad (25)$$

$$u_{k0}(z) = \frac{p_0 \sin(\beta_2 z)}{\mu_2 \beta_2 \cos(\beta_2 H)} - \frac{\mu_2 - \mu_1}{\mu_1} \frac{p_0 \cos(\beta_2 h)}{\mu_2 \Delta_{20}^I} G_{k0}(z, h), \quad (26)$$

Finally, applying the inverse finite Hankel transform (11) to this expression yields

$$u_k(r, z) = \frac{4rp_0}{\mu_2(R^4 - a^4)} \left[\frac{\sin(\beta_2 z)}{\beta_2 \cos(\beta_2 H)} - \frac{\mu_2 - \mu_1}{\mu_1} \frac{\cos(\beta_2 h)}{\Delta_{20}^I} G_{k0}(z, h) \right] + \frac{1}{\mu_2} \sum_{n=1}^{\infty} p_n \left[\frac{\sinh(\gamma_{2n} z)}{\gamma_{2n} \cosh(\gamma_{2n} H)} - \frac{\mu_2 - \mu_1}{\mu_1} \frac{\cosh(\gamma_{2n} h)}{\Delta_{2n}^I} G_{kn}(z, h) \right] \frac{K(\lambda_n, r)}{\|K(\lambda_n, r)\|^2}, \quad k = 1, 2. \quad (27)$$

This is the explicit expression for the displacements in the case of ideal contact. This can also be used to obtain the unique expression for the stress $\tau_{z\phi}^{(k)}$, $k = 1, 2$.

4.2. The displacement for soft coupling between the cylinders

Utilizing the transformed conditions for soft contact (15), the expressions for the displacements (20)-(21) can be written in the form

$$u_{kn}(z) = \frac{p_n \sinh(\gamma_{2n} z)}{\mu_2 \gamma_{2n} \cosh(\gamma_{2n} H)} - \left[K_1 \frac{\partial G_{kn}(z, \eta)}{\partial \eta} \Big|_{\eta=h} + \frac{\mu_2 - \mu_1}{\mu_1} G_{kn}(z, h) \right] u'_{2n}(h+0), \quad n \in \mathbb{N}, \quad (28)$$

$$u_{k0}(z) = \frac{p_0 \sin(\beta_2 z)}{\mu_2 \beta_2 \cos(\beta_2 H)} - \left[K_1 \frac{\partial G_{k0}(z, \eta)}{\partial \eta} \Big|_{\eta=h} + \frac{\mu_2 - \mu_1}{\mu_1} G_{k0}(z, h) \right] u'_{20}(h+0), \quad (29)$$

The unknown values $u'_{2n}(h+0)$ and $u'_{20}(h+0)$ are obtained using an almost identical procedure to that for the case of ideal contact. Namely, expressions (28)-(29) are differentiated with respect to variable z , and the substitutions $k = 2$ and $z = h + 0$ are made. The resulting linear algebraic equations for $u'_{2n}(h+0)$ are solved to yield

$$u'_{20}(h+0) = \frac{p_0 \cos(\beta_2 h)}{\mu_2 \Delta_{20}^S}, \quad u'_{2n}(h+0) = \frac{p_n \cosh(\gamma_{2n} h)}{\mu_2 \Delta_{2n}^S}, \quad (30)$$

where

$$\Delta_{20}^S = \cos(\beta_2 H) + \sin[\beta_2(H - h)] \left[K_1 \beta_2 \cos(\beta_2 h) + \frac{\mu_2 - \mu_1}{\mu_1} \sin(\beta_2 h) \right],$$

$$\Delta_{2n}^S = \cosh(\gamma_{2n}H) + \sinh[\gamma_{2n}(H-h)] \left[K_1 \gamma_{2n} \cosh(\gamma_{2n}h) + \frac{\mu_2 - \mu_1}{\mu_1} \sinh(\gamma_{2n}h) \right].$$

Inserting into (28)-(29), the explicit form of displacements in the transform domain is obtained

$$u_{kn}(z) = \frac{p_n \sinh(\gamma_{2n}z)}{\mu_2 \gamma_{2n} \cosh(\gamma_{2n}H)} - \left[K_1 \frac{\partial G_{kn}(z, \eta)}{\partial \eta} \Big|_{\eta=h} + \frac{\mu_2 - \mu_1}{\mu_1} G_{kn}(z, h) \right] \frac{p_n \cosh(\gamma_{2n}h)}{\mu_2 \Delta_{2n}^S}, \quad (31)$$

$$u_{k0}(z) = \frac{p_0 \sin(\beta_2 z)}{\mu_2 \beta_2 \cos(\beta_2 H)} - \left[K_1 \frac{\partial G_{k0}(z, \eta)}{\partial \eta} \Big|_{\eta=h} + \frac{\mu_2 - \mu_1}{\mu_1} G_{k0}(z, h) \right] \frac{p_0 \cos(\beta_2 h)}{\mu_2 \Delta_{20}^S}. \quad (32)$$

It can be seen that when constant $K_1 = 0$ the transformed displacements (31)-(32) coincide with those for the ideal contact subcase (25)-(26).

Applying the inverse finite Hankel transform (11) to the expressions for the transformed displacements (31)-(32) yields an explicit expression for the displacements in the case of soft contact

$$u_k(r, z) = \frac{4rp_0}{\mu_2(R^4 - a^4)} \left[\frac{\sin(\beta_2 z)}{\beta_2 \cos(\beta_2 H)} - \left(K_1 \frac{\partial G_{k0}(z, \eta)}{\partial \eta} \Big|_{\eta=h} + \frac{\mu_2 - \mu_1}{\mu_1} G_{k0}(z, h) \right) \frac{\cos(\beta_2 h)}{\Delta_{20}^S} \right] \\ + \frac{1}{\mu_2} \sum_{n=1}^{\infty} p_n \left[\frac{\sinh(\gamma_{2n}z)}{\gamma_{2n} \cosh(\gamma_{2n}H)} + \left(K_1 \frac{\partial G_{kn}(z, \eta)}{\partial \eta} \Big|_{\eta=h} + \frac{\mu_2 - \mu_1}{\mu_1} G_{kn}(z, h) \right) \frac{\cosh(\gamma_{2n}h)}{\Delta_{2n}^S} \right] \frac{K(\lambda_n, r)}{\|K(\lambda_n, r)\|^2}, \quad (33)$$

with $k = 1, 2$. This can again be utilized to obtain a unique expression for the stress $\tau_{z\phi}^{(k)}$, $k = 1, 2$.

4.3. The displacement for rigid coupling between the cylinders

Combining the transformed rigid contact conditions (17) with the assumed form of the displacement (20)-(21), the discontinuous problem for rigid contact is given by

$$u_{kn}(z) = \frac{p_n \sinh(\gamma_{2n}z)}{\mu_2 \gamma_{2n} \cosh(\gamma_{2n}H)} - \left[\frac{\mu_2 - \mu_1}{\mu_1} u'_{2n}(h+0) - K_2 \gamma_{0n}^2 u_{2n}(h+0) \right] G_{kn}(z, h), \quad (34)$$

$$u_{k0}(z) = \frac{p_0 \sin(\beta_2 z)}{\mu_2 \beta_2 \cos(\beta_2 H)} - \left[\frac{\mu_2 - \mu_1}{\mu_1} u'_{20}(h+0) + K_2 \beta_0^2 u_{20}(h+0) \right] G_{k0}(z, h), \quad (35)$$

We now seek the unknown values $u_{2n}(h+0)$ and $u'_{2n}(h+0)$ using same approach as in the two previous subcases. First the expressions (34)-(35) are

differentiated, followed by making the substitutions $k = 2$ and $z = h + 0$. The resulting system of linear algebraic equations for the unknown values $u_{2n}(h + 0)$ and $u'_{2n}(h + 0)$ are then solved for the cases $n = 0$ and $n \in \mathbb{N}$, yielding

$$\begin{aligned} u_{20}(h + 0) &= \frac{p_0 \sin(\beta_2 h)}{\mu_1 \Delta_{20}^R}, & u'_{20}(h + 0) &= \frac{p_0}{\mu_2 \Delta_{20}^R} [\beta_2 \cos(\beta_2 h) - K_2 \beta_0^2 \sin(\beta_2 h)], \\ u_{2n}(h + 0) &= \frac{p_n \sinh(\gamma_{2n} h)}{\mu_1 \Delta_{2n}^R}, & u'_{2n}(h + 0) &= \frac{p_n}{\mu_2 \Delta_{2n}^R} [\gamma_{2n} \cosh(\gamma_{2n} h) + K_2 \gamma_{0n}^2 \sinh(\gamma_{2n} h)], \end{aligned} \quad (36)$$

where $n \in \mathbb{N}$ and

$$\Delta_{20}^R = \beta_2 \cos(\beta_2 H) - \left[\frac{\mu_2 - \mu_1}{\mu_1} \beta_2 \sin[\beta_2(H - h)] + K_2 \beta_0^2 \cos[\beta_2(H - h)] \right] \sin(\beta_2 h),$$

$$\Delta_{2n}^R = \gamma_{2n} \cosh(\gamma_{2n} H) + \left[\frac{\mu_2 - \mu_1}{\mu_1} \gamma_{2n} \sinh[\gamma_{2n}(H - h)] + K_2 \gamma_{0n}^2 \cosh[\gamma_{2n}(H - h)] \right] \sinh(\gamma_{2n} h).$$

Inserting into (34)-(35), the transformed displacements are obtained

$$u_{kn}(z) = \frac{p_n \sinh(\gamma_{2n} z)}{\mu_2 \gamma_{2n} \cosh(\gamma_{2n} H)} - \frac{p_n}{\mu_2 \Delta_{2n}^R} \left[\frac{\mu_2 - \mu_1}{\mu_1} \gamma_{2n} \cosh(\gamma_{2n} h) - K_2 \gamma_{0n}^2 \sinh(\gamma_{2n} h) \right] G_{kn}(z, h), \quad (37)$$

$$u_{k0}(z) = \frac{p_0 \sin(\beta_2 z)}{\mu_2 \beta_2 \cos(\beta_2 H)} - \frac{p_0}{\mu_2 \Delta_{20}^R} \left[\frac{\mu_2 - \mu_1}{\mu_1} \beta_2 \cos(\beta_2 h) - K_2 \beta_0^2 \sin(\beta_2 h) \right] G_{k0}(z, h). \quad (38)$$

Note again that when the constant $K_2 = 0$ the derived solutions (37)-(38) coincide with those for the subcase of ideal contact (25)-(26).

Applying the inverse finite Hankel transform (11) to the transformed displacements (37)-(38) yields an explicit expression for the displacements

$$\begin{aligned} u_k(r, z) &= \frac{4rp_0}{\mu_2(R^4 - a^4)} \left[\frac{\sin(\beta_2 z)}{\beta_2 \cos(\beta_2 H)} - \frac{G_{k0}(z, h)}{\Delta_{20}^R} \left(\frac{\mu_2 - \mu_1}{\mu_1} \beta_2 \cos(\beta_2 h) - K_2 \beta_0^2 \sin(\beta_2 h) \right) \right] \\ &+ \frac{1}{\mu_2} \sum_{n=1}^{\infty} p_n \left[\frac{\sinh(\gamma_{2n} z)}{\gamma_{2n} \cosh(\gamma_{2n} H)} - \frac{G_{kn}(z, h)}{\Delta_{2n}^R} \left(\frac{\mu_2 - \mu_1}{\mu_1} \gamma_{2n} \cosh(\gamma_{2n} h) - K_2 \gamma_{0n}^2 \sinh(\gamma_{2n} h) \right) \right] \frac{K(\lambda_n, r)}{\|K(\lambda_n, r)\|^2}, \end{aligned} \quad (39)$$

where $k = 1, 2$. This can again be utilized to obtain a unique expression for the stress $\tau_{z\phi}^{(k)}$, $k = 1, 2$.

| | Height [m] | Density ρ [kg/m ³] | Shear modulus μ [Pa] | Wave-speed c [m/s] |
|------------------------------|------------|-------------------------------------|--------------------------|----------------------|
| Lower section (Cuprum) | 0.05 | 8900 | 40.70×10^9 | 2250 |
| Upper section (Aluminium) | | 2700 | 25.00×10^9 | 3110 |
| Soft interface | 0.01 | 5800 | 3.285×10^9 | 2680 |
| Rigid interface | 0.01 | 5800 | 3285×10^9 | 2680 |

Table 1: Material properties and geometry of the cylinder used in simulations for Sect. 5.1. The height of the upper cylinder is 0.05 [m] in the case of ideal contact, and 0.04 [m] in the case of a soft or rigid interface, to maintain a fixed total height $H = 0.1$ [m]. The hollow cylinders' inner radius is $a = 0.25$ [m], while the outer radius is $R = 0.5$ [m].

5. Numerical results for the displacement and stress

With this, the unique expressions for the displacements have been obtained for all three cases: ideal contact (27), soft contact (33), and rigid contact (39). The stress $\tau_{z\phi}^{(k)}$, $k = 1, 2$, then follows from the stress-displacement relations. The results below are computed using these formulae in a Python environment.

We consider the case where the two cylinder sections are comprised of cuprum (copper) and aluminium respectively. In the case of a soft or rigid interface, the interfacial layer is assumed to have height $h_0 = 0.01$ [m], while the shear modulus for soft interface is given by $\mu_{soft} = (\mu_1 + \mu_2)/200$, and for the rigid interface $\mu_{rigid} = 100(\mu_1 + \mu_2)/2$. The interface materials' density is taken as the average of the upper and lower cylinders $\rho_0 = (\rho_1 + \rho_2)/2$ for both soft and rigid contact. The resulting material parameters are provided in Table. 1. For the sake of convenience, in all simulations we consider the axisymmetric loading on the upper surface $z = H$ (2)₂ to be given by $p(r) = (1 - r^2)$, such that

$$\tau_{z\phi}^{(2)} \Big|_{z=H} = (1 - r^2)e^{i\omega t}. \quad (40)$$

Note that this is a steady-state loading to match the rotation of the cylinder, and as such the resulting stresses and displacements within the cylinder are independent of time t . In Sect. 5.1 - 5.2 we take $\omega = 1$ [Hz] for the sake of simplicity, while the impact of varying ω is considered in Sect. 5.3.

The authors also carried out simulations with other cylinder geometries and material compositions. These were found to match the general trends

reported in this section. We therefore only show results for the stated configuration, for the sake of brevity.

In Sect. 5.1, we consider the impact that the type of interface (ideal, soft or rigid) has on the resulting cylinder displacements and stresses. Then, in Sect. 5.2 we examine the impact of varying the shear modulus of the interface layer in the case of soft and rigid contact. Finally, the varying of rotation rates is considered in Sect. 5.3.

5.1. Impact of the interface on the system behaviour

Let's consider the change of displacements and stress inside a cylinder of fixed height $H = 0.1$ [m], inner radius $a = 0.25$ [m], and outer radius $R = 0.5$ [m]. The material properties of the coupled cylinder are listed in Table. 1, while the upper face is subject to the applied loading stated in (40).

We consider the scaled displacement $\mu_2 u(r, z)$ and stress $\tau_{z\phi}(r, z)$, at various fixed heights z within the cylinder. The results for $z/H = 0.25, 0.5, 0.75$ are provided in Fig. 2.

Let us consider the behaviour observed within each section of the coupled cylinder separately.

In the lower cylinder (Fig. 2a,b) the displacement and stress for the case of soft and rigid contact are almost identical. Meanwhile, the ideal contact condition gives rise to a slightly different profile. This is seen most clearly for the tangential stress, which experiences a higher stress over the whole plane, while also having a less linear profile over r . The overall impact of the assumed contact condition on the displacement is however only marginal for the lower cylinder, most likely due to the assumed torsion loading taking place at the top of the cylinder $z = H$.

For the middle of the cylinder (Fig. 2c,d), which marks the start of the interface, the impact of the assumed contact condition on the displacement is far more substantial. The case of soft contact yields a significantly higher displacement than that for the ideal or rigid conditions, but a significantly lower tangential stress. Meanwhile, the results for ideal and rigid contact conditions are very close to one another, with only a small (but still visible) difference for the displacement and stress.

The displacements in the middle of the upper cylinder (Fig. 2e,f) display a similar trend to that for the interface. The soft contact condition leads to a significantly higher displacement but lower tangential stress compared to the ideal and rigid conditions, although the relative difference in the stresses is smaller than seen at the interface (due to the fact that the tangential loading

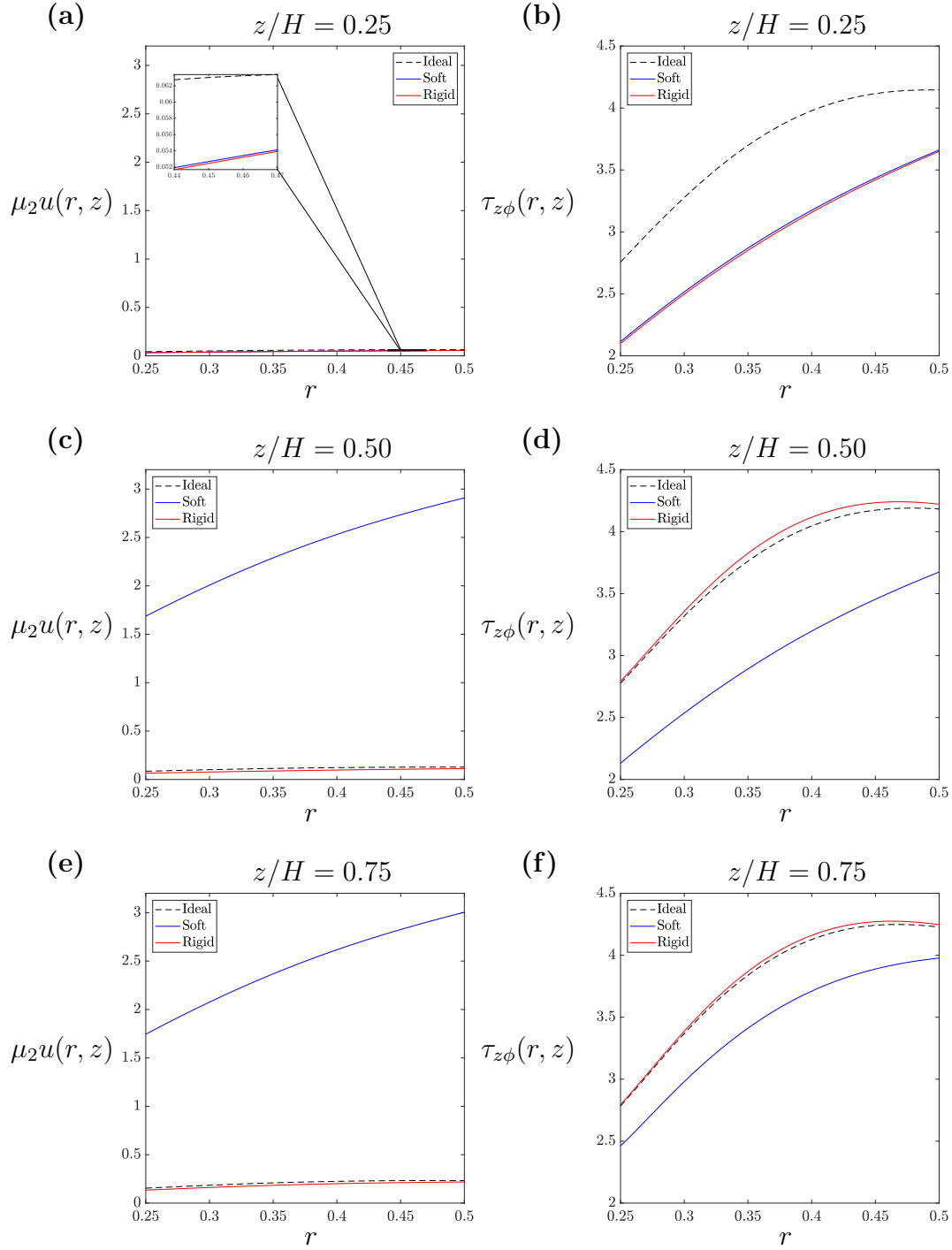


Figure 2: The change of (a), (c), (e) the scaled displacement and (b), (d), (f) the stress for various fixed heights in a coupled cuprum-aluminium cylinder with an ideal, soft or rigid interface between the sections. We show the fixed heights: (a), (b) the middle of the lower (cuprum) cylinder $z/H = 0.25$, (c), (d) the (start of the) interface $z/H = 0.5$, (e), (f) (near) the middle of the upper (aluminium) cylinder $z/H = 0.75$.

is occurring at the top of the cylinder $z = H$). Meanwhile, the displacement and tangential stress for ideal and rigid contact are very similar, although the difference between them is still noticeable.

We can also consider the dependence of the displacement and stress on the radial position r .

In all vertical positions within the cylinder shown in Fig. 2, we can see that displacement exhibits almost linear behaviour over r . Meanwhile, in the lower cylinder ($z/H = 0.25$), we can see that the soft and rigid interfaces exhibit almost linear behaviour of the tangential stress over r , while that for the ideal interface is less linear (although is still monotonic). However, at the interface ($z/H = 0.5$) only the soft interface experiences near linear behaviour over r . In the upper cylinder ($z/H = 0.75$) the tangential stress behaves nonlinearly for all coupling conditions, and the cases with ideal and rigid interfaces are no longer monotonic over r .

Investigations by the authors have shown that almost-linear behaviour dominates in the case where the ratio of cylinder outer radius to height $R/H < 5$. Conversely, when taking $R/H \geq 5$ a clearly nonlinear pattern emerges for the displacement and stress. This motivates further investigation of the impact of this ratio on the behaviour for each from of interfacial coupling.

5.2. Impact of varying the cylinder geometry and composition

With the general behaviour of the displacement and stress for the different interface conditions considered, let us now examine how varying the interface composition and cylinder geometry impacts the results.

Namely, for the simulations in this section we consider cylinders' with lower cylinder shear modulus $\mu_1 = 10^9$ [Pa], and upper cylinder $\mu_2 = 2 \times 10^9$ [Pa], and vary the ratio of the interface shear modulus μ_0/μ_1 in the case of soft or rigid contact by varying the interface shear modulus μ_0 . The density of each section ρ_0, ρ_1, ρ_2 and interface height h_0 are taken in line with those from Sect. 5.1 (see Table. 1). These are considered for cylinders with fixed height $H = 0.1$ [m], while varying the outer radius $R = 0.05, 0.25, 0.5$ [m] to obtain ratios $R/H = 0.5, 2.5, 5.0$. The inner radius in each case is taken as $a = R/2$ [m]. We investigate how these various configurations impact the relative difference of the displacement and stress at a fixed point in the radial centre $r = (R + a)/2$ at the start of the interface $z = h$, compared to the case of ideal contact conditions

Relative difference between ideal and rigid contact

| | | μ_0/μ_1 | | | |
|---------------------|-------|---------------|----------|----------|----------|
| | | 10.0 | 50.0 | 100.0 | |
| Displacement | R/H | 0.5 | 0.002160 | 0.004938 | 0.005884 |
| | | 2.5 | 0.065772 | 0.163634 | 0.201234 |
| | | 5.0 | 0.062962 | 0.180386 | 0.237041 |

| | | μ_0/μ_1 | | | |
|---------------|-------|---------------|----------|----------|----------|
| | | 10.0 | 50.0 | 100.0 | |
| Stress | R/H | 0.5 | 0.004433 | 0.010135 | 0.012076 |
| | | 2.5 | 0.016629 | 0.040485 | 0.049558 |
| | | 5.0 | 0.005923 | 0.014839 | 0.018881 |

Table 2: Relative difference between the cases of ideal and rigid contact for the (a) displacement $u(r, z)$, (b) tangential stress $\tau_{z\phi}(r, z)$, at the start of the cylinders' interface $z = h$ and the radial centre of the hollow cylinder $r = (R + a)/2$. Three values of soft interface shear modulus μ_0 are considered, while the upper and lower cylinder shear moduli $\mu_1 = 10^9$ [Pa], $\mu_2 = 2 \times 10^9$ [Pa], are kept fixed between simulations. Results are shown for varying cylinder width-height ratio R/H , where $H = 0.1$ [m] is the (fixed) total height of the cylinder, while outer radius R is varied, and the inner radius is taken as $a = R/2$ [m].

The relative difference between the case of ideal contact and that with a rigid interface layer is provided in Table. 2. It can again be seen that there is a close correspondence between these cases (as previously shown graphically in Fig. 2), with the final relative difference between them depending on both the interface ratio μ_0/μ_1 and the width-height ratio R/H . The difference in the tangential stress between ideal contact and the rigid interface is close to 1% for the cases $R/H = 0.5, 5.0$, for all values of the shear modulus ratio μ_0/μ_1 . Interestingly, there is a value of R/H for which the relative difference in the tangential stress between rigid and ideal contact is maximised at the interface $z = h$, with the relative differences for $R/H = 2.5$ being consistently higher than those for $R/H = 0.5$ or $R/H = 5$, reaching almost 5% when $\mu_0/\mu_1 = 100$. The relative differences in the displacement meanwhile behaves monotonically, increasing with both R/H and μ_0/μ_1 . While the difference is small for the case of a long, thin cylinder ($R/H = 0.5$) - never exceeding 0.6% - the case of a short, fat cylinder ($R/H = 5.0$) sees a

Relative difference between ideal and soft contact

| | | μ_0/μ_1 | | | |
|--------------|-------|---------------|----------|---------|---------|
| Displacement | R/H | | 0.1 | 0.05 | 0.01 |
| | | 0.5 | 0.651907 | 1.30039 | 6.47525 |
| | | 2.5 | 2.88752 | 5.49900 | 25.0973 |
| | | 5.0 | 5.78273 | 10.8609 | 46.6705 |
| | | | | | |

| | | μ_0/μ_1 | | | |
|--------|-------|---------------|----------|----------|----------|
| Stress | R/H | | 0.1 | 0.05 | 0.01 |
| | | 0.5 | 0.011179 | 0.015338 | 0.021838 |
| | | 2.5 | 0.117186 | 0.166791 | 0.252894 |
| | | 5.0 | 0.109589 | 0.166652 | 0.290020 |
| | | | | | |

Table 3: Relative difference between the cases of ideal and soft contact for the (a) displacement $u(r, z)$, (b) tangential stress $\tau_{z\phi}(r, z)$, at the start of the cylinders' interface $z = h$ and the radial centre of the hollow cylinder $r = (R + a)/2$. Three values of soft interface shear modulus μ_0 are considered, while the upper and lower cylinder shear moduli $\mu_1 = 10^9$ [Pa], $\mu_2 = 2 \times 10^9$ [Pa], are kept fixed between simulations. Results are shown for varying cylinder width-height ratio R/H , where $H = 0.1$ [m] is the (fixed) total height of the cylinder, while outer radius R is varied, and the inner radius is taken as $a = R/2$ [m].

relative difference of the displacement as high as 24%.

Next, the relative difference between the case of ideal contact and that with a soft interface layer is provided in Table. 3. There is again a clear difference in behaviour between the soft interface and that for ideal or rigid contact. There is a monotonic increase in the relative difference of the displacement with increasing width-height ratio R/H and shear moduli ratio μ_0/μ_1 . The differences are however far larger than those for the comparison of rigid and ideal contact conditions, with the minimum relative difference of the displacement at $z = h$ being 65%, and the maximum exceeding 4667%. Note that this exceptionally high value is due to the cylinder material composition, geometry, and very low shear modulus of the soft layer - with the value in the other considered cases being far lower. Meanwhile, the relative difference of the tangential stress increases monotonically with decreasing shear moduli ratio μ_0/μ_1 , but follows a more complicated pattern with varying width-height ratio R/H . When $\mu_0/\mu_1 = 0.1, 0.05$ there is a maximum

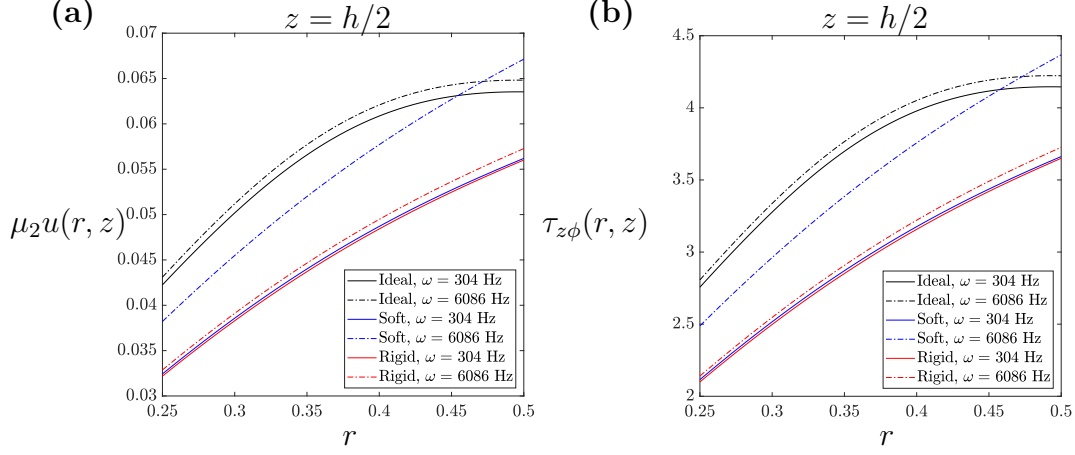


Figure 3: The change of (a) the scaled displacement and (b) the stress in a coupled aluminium-cuprum cylinder subject to differing rotation rates ω with an ideal, soft or rigid interface between the upper and lower cylinders. All values are taken at the fixed height $z = h/2$ (middle of the lower cylinder).

of the relative difference (compare $R/H = 2.5$ with $R/H = 0.5, 5.0$), however it behaves monotonically with R/H when $\mu_0/\mu_1 = 0.01$. Regardless, in all cases the relative difference of the tangential stress between the soft and ideal contact conditions are significantly larger than those for the rigid-ideal comparison, with the minimum again being about 1%, but the maximum exceeding 29% at the interface $z = h$.

5.3. Impact of varying the cylinder rotation rate

In the proceeding subsections we kept a fixed cylinder rotation rate $\omega = 1$ [Hz]. Now, let us vary the rotation rate, and examine the impact on the stress and displacement for the three types of coupled interface.

We again consider an aluminium-cuprum cylinder that has height $H = 0.1$ [m], with the interface between the aluminium and cuprum sections beginning at height $h = 0.05$ [m]. Both sections have inner radius $a = 0.25$ [m] and outer radius 0.5 [m] (see Table. 1). The loading on the upper face of the cylinder is also unchanged $p(r) = 1 - r^2$. The results provided below are however general to all cylinder geometries and material compositions considered by the authors.

Results for the differing interfacial layers (ideal, soft, rigid) under two differing rotation rates are provided in Fig. 3. Note that these correspond to the same height as shown in Fig. 2a,b (for $\omega = 1$ [Hz]). The rotation rates

in Fig. 3 are chosen such that the natural normalisation $\tilde{\omega} = \omega H / \sqrt{\mu_2 / \rho_2}$ takes values $\tilde{\omega} = 0.01$ and $\tilde{\omega} = 0.2$.

As would be expected, increasing the rotation rate leads to an outwards (positive) displacement and tangential stress. Comparing Fig. 2a,b with Fig. 3, it is clear that the effect is only marginal when going from $\omega = 1$ [Hz] to $\omega = 304$ [Hz], but becomes far more significant when increasing to $\omega = 6086$ [Hz]. The magnitude of this effect is also significantly larger in the case of a soft interface, compared to that for the ideal and rigid interfacial layer.

6. Using an interfacial layer to approximate damage within a cylinder

The presented formulation and solutions for the displacement allows for modelling a coupled cylinder with various interfacial coupling conditions. However, it may also be possible to use this to approximate damage at height $z = h$ within a single cylinder, such as the presence of a hidden ring crack. This can be achieved by considering a weak interface at $z = h$, which mimics the reduced bonding between the parts of the cylinder above and below the damaged region. Such an approximation can be created provided some link between the effect of the damage and the shear modulus of the interfacial layer can be obtained.

Let us consider a cylinder whose upper and lower sections are both comprised of the same material, such that $\rho_1 \equiv \rho_2$ and $\mu_1 \equiv \mu_2$. To allow for comparison with the previous paper Zhuravlova et al. (2024), we consider a small cylinder whose upper and lower sections are made of steel, with some soft interface between them having height $h_0 = 10^{-4}$ [m] (mimicking the ring crack in the stated paper). The cylinder has inner radius $a = 5.5 \times 10^{-3}$ [m], outer radius $R = 7.5 \times 10^{-3}$ [m], and height $H = 5 \times 10^{-3}$ [m]. Note that the comparison between the model presented here and the work of Zhuravlova et al. (2024) is not perfect, as that paper assumes loading applied to the inner walls of the cylinder $r = a$ while here we assume loading on the upper face of the cylinder $z = H$, however this will not significantly impact the result.

We consider the displacement $u(r, z)$ at the top of the cylinder $z = H$, as that where measurements are most easily taken in practical applications. Let us investigate the ratio of the displacements between the cylinder with a soft interface and the ideal case $u_{soft}(r, H) / u_{ideal}(r, H)$. Note that in practical application this would correspond to the observed displacement divided by

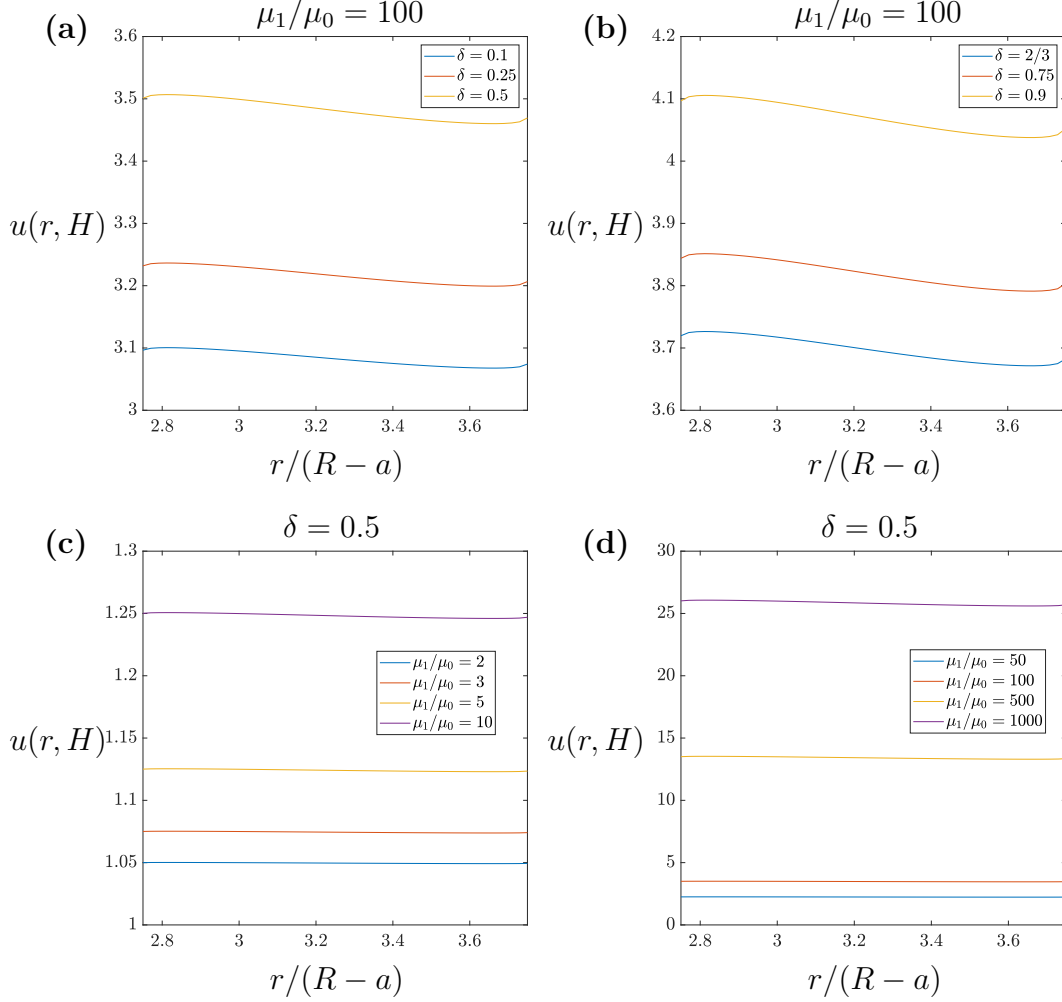


Figure 4: The displacement at the top of the cylinder $u(r, H)$ for: (a), (b) fixed shear moduli ratio $\mu_1/\mu_0 = 100$ and varying relative interface height $\delta = h/H$; (c), (d) fixed relative interface height $\delta = 0.5$ and varying shear moduli ratio μ_1/μ_0 .

that predicted for a cylinder without an interfacial layer. This ratio for various relative interface positions $\delta = h/H$ and shear moduli ratio μ_1/μ_0 are provided in Fig. 4. It can be seen that the interface position and shear moduli ratio both play a key role in determining the magnitude of the resulting displacement. However, the distribution of that displacement over r is only small compared to the magnitude of the displacement.

Consequently, it makes sense to consider the arithmetic mean of the dis-

placement ratio over radial points $r = [r_1, \dots, r_N]$ which, noting (27), (33), the formulae for the Green's function (18), (19), the definition of K_1 , and that $\mu_1 \equiv \mu_2$, $c_1 \equiv c_2$ (so $\beta_1 \equiv \beta_2$, $\gamma_{1n} \equiv \gamma_{2n}$), is given by

$$\begin{aligned}\bar{u} &= \frac{1}{N} \sum_{i=1}^N \frac{u_{soft}(r_i, H)}{u_{ideal}(r_i, H)} \\ &= 1 + \frac{\mu_1 h_0}{\mu_0 N} \sum_{i=1}^N \frac{\frac{4r_i p_0}{R^4 - a^4} \frac{\cos(\beta_2 h)}{\cos(\beta_2 H)} \frac{\cos(\beta_2 h)}{\Delta_{20}^S} - \sum_{n=1}^{\infty} p_n \frac{\cosh(\gamma_{2n} h)}{\cosh(\gamma_{2n} H)} \frac{\cosh(\gamma_{2n} h)}{\Delta_{2n}^S} \frac{K(\lambda_n, r_i)}{\|K(\lambda_n, r_i)\|^2}}{\frac{4r_i p_0}{\beta_2(R^4 - a^2)} \tan(\beta_2 H) + \sum_{n=1}^{\infty} \frac{p_n}{\gamma_{2n}} \tanh(\gamma_{2n} H) \frac{K(\lambda_n, r_i)}{\|K(\lambda_n, r_i)\|^2}},\end{aligned}\quad (41)$$

where in this special case $\mu_1 \equiv \mu_2$, $c_1 \equiv c_2$

$$\Delta_{20}^S = \cos(\beta_2 H) + \frac{\mu_1 h_0}{\mu_0} \beta_2 \sin[\beta_2(H - h)] \cos(\beta_2 h),$$

$$\Delta_{2n}^S = \cosh(\gamma_{2n} H) + \frac{\mu_1 h_0}{\mu_0} \gamma_{2n} \sinh[\gamma_{2n}(H - h)] \cosh(\gamma_{2n} h).$$

This expression indicates an almost linear relationship between the shear modulus ratio μ_1/μ_0 and the arithmetic mean displacement ratio \bar{u} . This is confirmed in Fig. 5, with least-squares analysis revealing that for the given material parameters and cylinder geometry \bar{u} can be accurately described by (to 4 significant figures)

$$\bar{u} = 1.000 + 0.02482 \frac{\mu_1}{\mu_0}.$$

In fact, this linear approximation yields a relative error below 0.01% for all of the points computed, which is of comparable order to the accuracy of computations. It should be noted however that the weak interface assumptions mean that the error will be slightly higher in the limit $\mu_1/\mu_0 \rightarrow 1$ as the right-hand side of (41) doesn't go to zero (we have $\bar{u} \rightarrow 1.02$ rather than $\bar{u} \rightarrow 1.00$, to three significant figures). However, given that we would assume $\mu_0 < \mu_1$ in the case of a damaged cylinder, this means that the linear approximation can be used in all relevant cases.

This provides a convenient method of determining the appropriate interface shear modulus μ_0 to properly approximate the damaged cylinder. Namely, choosing μ_0 based on the known magnitude of the arithmetic mean of the displacement ratio \bar{u} , the location at which the damage occurs h , and the height of the damaged region h_0 , based on a linear approximation of (41).

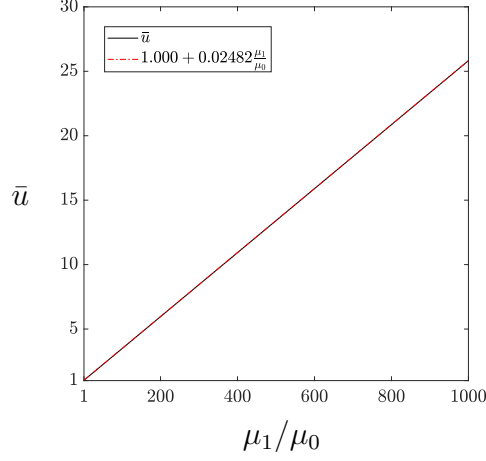


Figure 5: The arithmetic mean over r of the displacement ratio u_{soft}/u_{ideal} (41) at the interface $z = h$, alongside a linear approximation produced using the least-square method. Results are for a steel cylinder with fixed interface relative height $\delta = h/H = 0.5$.

One additional benefit of the weak interface approximation comes from a crucial difference between the displacement observed for the weak interface and that when a ring crack is present. Namely, the profile over r of the displacement ratio compared to the ideal case $u_{soft}(r, h)/u_{ideal}(r, h)$. As seen in Fig. 4, the weak interface provides an almost constant displacement ratio over r , due to the impact on the bonding between the upper and lower cylinders being equally spread across the entire interface. In the previous work by the authors however Zhuravlova et al. (2024), it was demonstrated that a ring crack with produce significant variation in the displacement over r - most notably the clear presence of a maximum (see Fig. 4 in that paper). Therefore, the weak interface approximation allows for a simple method of approximating the relative magnitude of the displacement, while the distribution of the displacement across the cylinder provides a non-destructive test to infer the type of damage present (e.g. whether or not a crack is forming) and the proportion of the ‘interface’ that it covers.

7. Summary and concluding remarks

The torsion problem of a coupled hollow cylinder subject to various forms of coupling between the upper and lower cylinders’ (ideal, soft, rigid) was considered. The cylinders were of arbitrary geometry and torsion loading on

the upper face, while the bottom was fixed in place and the cylinder' sides assumed free from loading. The solution for the displacement and tangential stress in each case were obtained in terms of the Green's function, utilizing the finite Hankel transform.

The results of simulations demonstrated a number of key trends:

- There is a close correspondence between the results for the ideal and rigid interface, although there is some difference in behaviour near the bottom of the cylinder (see Fig. 2a,b). Between these two cases, the relative difference in the displacement at the interface remained below 0.6% for the long thin cylinder ($R/H = 0.5$) for all shear moduli ratios μ_0/μ_1 , and below 7% for the modest shear ratio $\mu_0/\mu_1 = 10$, but could rise as high as 24% for short fat cylinders ($R/H \geq 2.5$) with extreme shear moduli ratios (see Table. 2). Meanwhile, the relative difference in the tangential stresses was $< 5\%$, for all simulated shear moduli and cylinder geometries.
- There is a clear difference in behaviour between the soft interface and that for ideal or rigid contact, with a relative difference of the displacement at the interface between 65% - 4667%, depending on the cylinder geometry and interface material, although the relative difference in the tangential stress is far smaller (see Table. 3). There is however a close correspondence in the displacement and stress between the soft and rigid interfaces at the bottom of the cylinder (see Fig. 2a,b).
- The impact of rotation frequency ω on the cylinder displacement and tangential stress is relatively small compared to that of changing the shear modulus and cylinder geometry. The effect is however far more significant for the case of a soft contact condition than for the ideal or rigid case (see Fig. 3).
- The impact of the particular torsion loading on the displacement depends primarily upon the magnitude of the torsion loading, with some weighting towards loads applied towards the outer cylinder edge $r = R$ (see the form and impact of p_n (12) on the displacement (27), (33), (39)).

The results for the stress and displacement obtained in this work can be directly applied when considering the construction of coupled cylinders

in application. For example, determining whether a weak or hard adhesive between sections will best achieve the desired system properties.

The presented model may also be used to approximate damage within a single cylinder. This is achieved by approximating the damaged region using a weak interface, with the method for doing so being outlined in Sect. 6. If some mean difference in the displacement ratio \bar{u} (between the ideal/‘expected’ displacement and that measured) at the top of the cylinder is detected, and the damage is believed to start at $z = h$ and have height h_0 , then a linear approximation of (41) can be used to determine the appropriate interface shear modulus μ_0 for the approximation. The displacement then follows easily from (33). Further, the variation of the displacement over r measured at the top of the cylinder can be used to infer the type of damage present, as it is directly linked to the extent of bonding between the regions above and below the damaged area. If there is little variation over r then there is likely almost uniform damage over the damaged area, while the presence of notable maxima may indicate a ring crack (see Zhuravlova et al. (2024), Fig. 4).

It should be noted that throughout this work we have assumed the rotational frequency of the cylinder $\omega \neq 0$. When considering the case where the frequency $\omega = 0$, the systems governing equation reduces to the Laplacian $\Delta u_k = 0$ within each cylinder $k = 1, 2$. The model presented in this work can therefore be used to describe a range of other problems, such as the heat flux across a pair of joined cylinders, with applications to geothermal wells, amongst others. This could be further improved through the inclusion of thermoelastic effects within the model, in particular with regards to the interface. This will be the subject of future work by the authors.

CRediT authorship contribution statement

Igor Istenes initiated the research, contributed ideas, analysis of results. **Daniel Peck** analysis of results, visualisation, produced the manuscript. **Yuriy Protserov** contributed ideas, analysis of results. **Natalya Vaysfeld** contributed ideas, analysis of results, reviewed/edited the manuscript. **Zinaida Zhuravlova** performed the derivations, initial visualisation, analysis of results, produced the code, produced the manuscript, oversaw all research.

Acknowledgements

All authors were supported under European project funded by Horizon 2020 Framework Programme for Research and Innovation (2014–2020) (H2020-MSCA-RISE-2020) Grant Agreement number 101008140 EffectFact “Effective Factorisation techniques for matrix-functions: Developing theory, numerical methods and impactful applications”. D. Peck acknowledge supports from a project within the Innovate Ukraine competition, funded by the UK International Development and hosted by the British Embassy Kyiv. N. Vaysfeld acknowledges support from the Royal Society Wolfson Visiting Fellowship R3/233003.

References

- Akbarov, S., Bagirov, E., and Ipek, C. (2025). Influence of imperfect contact condition on dispersion of axisymmetric waves in bi-layered hollow cylinder with inhomogeneous initial stresses. *International Applied Mechanics*, 60(6):758–767.
- Akbarov, S., Kepceler, T., and Mert Egilmez, M. (2011). Torsional wave dispersion in a finitely pre-strained hollow sandwich circular cylinder. *Journal of Sound and Vibration*, 330(18):4519–4537.
- Akhmedov, N. and Ustinov, Y. A. (2009). Analysis of the structure of the boundary layer in the problem of the torsion of a laminated spherical shell. *Journal of Applied Mathematics and Mechanics*, 73(3):296–303.
- Argatov, I. and Mishuris, G. (2011). Frictionless elliptical contact of thin viscoelastic layers bonded to rigid substrates. *Applied Mathematical Modelling*, 35(7):3201–3212.
- Bigoni, D., Serkov, S., Valentini, M., and Movchan, A. (1998). Asymptotic models of dilute composites with imperfectly bonded inclusions. *International Journal of Solids and Structures*, 35(24):3239–3258.
- Dastjerdi, S., Malikan, M., Tahani, M., Kadkhodayan, M., and Ameli, A. (2025). On three-dimensional dynamics of smart rotating micro-disks. *International Journal of Engineering Science*, 211:104236.

- Dhua, S., Nath, A., and and, A. M. (2025). Effects of surface–interface theory on the circumferential shear horizontal wave in a piezoelectric composite cylinder. *Mechanics of Advanced Materials and Structures*, 0(0):1–22.
- Esfandyari, H. and Nejad, M. Z. (2025). Elastic analysis of uniform pressurized axisymmetric cylindrical shells made of saturated porous materials. *Results in Physics*, page 108194.
- Falope, F. O., Lanzoni, L., and Tarantino, A. M. (2025). Experiments on the finite torsion of nearly incompressible rubber-like materials: Nonlinear effects, analytic modeling and rubber characterization. *International Journal of Engineering Science*, 211:104254.
- Korenev, B. (2002). *Bessel Functions and Their Applications*. CRC Press, London.
- Kuo, Y. and Conway, H. (1973). The torsion of composite tubes and cylinders. *International Journal of Solids and Structures*, 9(12):1553–1566.
- Li, Y.-D., Zhao, H., and Xiong, T. (2013). The cylindrical interface crack in a layered tubular composite of finite thickness under torsion. *European Journal of Mechanics - A/Solids*, 39:113–119.
- Lipton, R. and Vernescu, B. (1996). Composites with imperfect interface. *Proceedings: Mathematical, Physical and Engineering Sciences*, 452(1945):329–358.
- Martynenko, N. and Pustilnikov, L. (1996). Finite integral transforms and their application to investigation of the systems with distributed parameters (in russian). *Moscow: Nauka*, 304(1986).
- Mikhasev, G. I. and Eremeyev, V. A. (2024). Effects of interfacial sliding on anti-plane waves in an elastic plate imperfectly attached to an elastic half-space. *International Journal of Engineering Science*, 205:104158.
- Mishuris, G. (2004a). Imperfect transmission conditions for a thin weakly compressible interface. 2d problems. *Archives of Mechanics*, 56:103–115.
- Mishuris, G., Movchan, N., and Movchan, A. B. (2006). Steady-state motion of a mode-iii crack on imperfect interfaces. *Quarterly Journal of Mechanics and Applied Mathematics*, 59:487–516.

- Mishuris, G. S. (2004b). Mode iii interface crack lying at thin nonhomogeneous anisotropic interface. asymptotics near the crack tip. In Movchan, A. B., editor, *IUTAM Symposium on Asymptotics, Singularities and Homogenisation in Problems of Mechanics*, pages 251–260, Dordrecht. Springer Netherlands.
- Pathak, R. S. and Singh, O. P. (1982). Finite Hankel transforms of distributions. *Pacific Journal of Mathematics*, 99(2):439–458.
- Popov, G., Abdimanov, S., and Ephimov, V. (1999). *Green’s functions and matrixes of the one-dimensional boundary problems (in Russian)*. Raczah, Almati.
- Protserov, Y. and Vaysfeld, N. (2017). Torsion problem for elastic multilayered finite cylinder with circular crack. *Applied Mathematics and Mechanics*, 38(3):423–438.
- Vaysfeld, N. and Protserov, Y. (2017). Torsion problems of finite cylinders weakened by ring-shaped cracks. *Procedia Structural Integrity*, 3:526–544.
- Wang, X. and Gong, Y. (1992). An elastodynamic solution for multilayered cylinders. *International Journal of Engineering Science*, 30(1):25–33.
- Zhuravlova, Z., Istenes, I., Peck, D., Protserov, Y., and Vaysfeld, N. (2024). Hidden ring crack in a rotating hollow cylinder under torsion. *International Journal of Engineering Science*, 194:103976.
- Zingerman, K. M., Zubov, L. M., Belkin, A. E., and Biryukov, D. R. (2023). Torsion of a multilayer elastic cylinder with sequential attachment of layers with multiple superposition of large deformations. *Continuum Mechanics and Thermodynamics*, 35:1235–1244.